Next Materials xxx (xxxx) xxx

Contents lists available at ScienceDirect

Next Materials

journal homepage: www.sciencedirect.com/journal/next-materials

Optimization of anodizing parameters for the morphological properties of TiO_2 nanotubes based on response surface methodology

Md. Arif Hossen [a,b], Azrina Abd Aziz [a,c,*], Riyadh Ramadhan Ikreedeegh [d,e], Aamina Din Muhammad [a], Nurashikin Yaacof [a], Kah Hon Leong [f], Lihua Wu [g]

[a] Faculty of Civil Engineering Technology, Universiti Malaysia Pahang Al-Sultan Abdullah, 26300 Kuantan, Pahang, Malaysia
[b] Center for Environmental Science & Engineering Research (CESER), Chittagong University of Engineering & Technology, 4349 Chattogram, Bangladesh
[c] Center for Advanced Intelligent Materials, Universiti Malaysia Pahang Al-Sultan Abdullah, 26300 Kuantan, Pahang, Malaysia
[d] Department of Analysis and Quality Control, Sarir Oil Refinery, Arabian Gulf Oil Company, P.O. Box 263, Benghazi, Libya
[e] Libyan Advanced Center for Chemical Analysis, Tripoli, P.O. Box 80851, Libya
[f] Department of Environmental Engineering, Faculty of Engineering and Green Technology, Universiti Tunku Abdul Rahman, 31900 Kampar, Perak, Malaysia
[g] Kuantan Sunny Scientific Collaboration Sdn. Bhd., Jalan Imbi, 55100 Kuala Lumpur, Malaysia

ARTICLE INFO

Keywords:
Titania nanotubes
Anodic oxidation
Morphology
RSM
Anodization parameters

ABSTRACT

TiO_2 nanotube (TNT) morphology is crucial for applications in a variety of fields. In this paper, response surface methodology (RSM) has been utilized to optimize the anodizing parameters i.e., electrolyte concentration (C), anodization voltage (V), and time (t) for morphology (e.g., nanotube diameter and length) of TNTs. Ethylene glycol (EG) based electrolyte has been used for anodization employing ammonium fluoride (NH_4F) as a source of fluoride ion (F^-) with 2.5 vol% H_2O. Reliable regression models have been developed between the input variables and the corresponding responses, namely tube diameter and length with multiple regression coefficients of 0.9649 and 0.9253, respectively, revealing a trustworthy association between the actual and those predicted values using the quadratic model. The predicted values of C (0.31 wt%), V (38.44 V), and t (69.37 min) were found to be the optimum anodization condition preceding a TiO_2 nanotubes diameter of 99.31 nm and length of 4572.64 nm. It was observed that the nanotubes diameter and length are more affected by anodizing voltage and time, and less sensitive to NH_4F concentration. Therefore, RMS could be an appropriate technique to optimize anodizing parameters for producing TiO_2 nanotubes with good morphology.

1. Introduction

Titanium dioxide (TiO_2) nanotube arrays have attracted great interest since they were discovered in 1984 by Assefpour-Dezfuly and coworkers [1]. Generally, TiO_2-based nanomaterials are known for their availability, non-toxicity, low cost, corrosion resistance, strong redox ability, and high chemical and thermal stability [2–6]. Compared to their bulk counterparts, the one-dimensional (1-D) highly ordered TiO_2 nanotube arrays (TNTs) possess unique architectural properties due to their high surface-to-volume ratios which facilitate the flow of electrons among the nanotube walls and offer more scattering and trapping of light [7–9]. Therefore, the TNTs have been widely used in many applications including photocatalysis [10–13], gas sensing [14,15], solar cells [16,17], and biomedical devices [18–20].

There are several synthetic approaches that could be used to fabricate highly organized TiO_2 nanotubular structures such as template-assisted technique, solvothermal treatment, hydrothermal treatment, and electrochemical anodization [21]. Among all these synthesis methods, the electrochemical anodization using an ethylene glycol/ammonium fluoride electrolyte is considered the most commonly adapted route due to its simplicity, low cost, versatility, and good controllability over morphology [22,23]. The TNTs performance in their different applications is greatly dependent on the surface area of the nanotubes which can be increased by modifying the morphologies of these nanotubes. However, there are some factors that can greatly influence the morphology, especially the diameter and length of TiO_2 nanotubes. These factors include the three main operating parameters of electrolyte concentration, anodization voltage, and anodization time [23–25].

Hitherto, a substantial number of studies have been conducted on the

* Corresponding author at: Faculty of Civil Engineering Technology, Universiti Malaysia Pahang Al-Sultan Abdullah, 26300 Kuantan, Pahang, Malaysia.
E-mail address: azrinaaziz@ump.edu.my (A. Abd Aziz).

https://doi.org/10.1016/j.nxmate.2023.100061
Received 14 August 2023; Received in revised form 23 October 2023; Accepted 6 November 2023

Table 1
Control variables and their respective levels.

Control variables	Coded symbols	Levels				
		-α	Low (−1)	Mid (0)	High (1)	+α
NH_4F conc. (wt %)	X_1	0.23	0.3	0.4	0.5	0.57
Anodization voltage (V)	X_2	6.36	20	40	60	73.65
Anodization time (min.)	X_3	19.20	60	120	180	220.90

Table 2
Central composite design parameters and results for the response variables nanotubes inner diameter (D) and length (L).

Run No.	Experimental variables			Response variables	
	Concentration (X_1)	Voltage (X_2)	Time (X_3)	Diameter (nm)	Length (nm)
01	0.4	40	120	110.9	5614.2
02	0.4	40	120	115.8	6123.8
03	0.3	60	180	30.1	3201.4
04	0.57	40	120	91.3	4191.6
05	0.3	20	60	31.8	1962.8
06	0.4	40	120	108.7	5321.6
07	0.5	20	180	49.3	4281.7
08	0.23	40	120	98.7	4239.2
09	0.4	73.65	120	42.6	3707.8
10	0.5	60	60	98.4	4844.6
11	0.3	20	180	52.3	3931.8
12	0.4	40	120	110.4	5529.3
13	0.4	40	120	112.6	5838.4
14	0.3	60	60	102.4	5281.3
15	0.5	20	60	41.2	1523.5
16	0.4	6.36	120	20.3	1123.5
17	0.4	40	120	108.8	5291.7
18	0.4	40	220.90	52.8	5541.5
19	0.4	40	19.10	80.8	3426.7
20	0.5	60	180	32.7	3027.2

influence of anodization parameters on the growth of TiO_2 nanotubes [24–28]. In 2018, Ozkan and coworkers [24] investigated the influence of the anodization parameters (applied voltage, composition of electrolyte, anodization time, and temperature) on the TiO_2 nanotube formation and tube-to-tube spacing. It was found that the TNT morphology changes from porous to spaced tubular layers at higher voltages. On the other hand, it was observed that the temperature and water content have an inverse relation with the tube-to-tube spacing. Tesler et al. [25] have similarly examined the effect of anodization parameters on the TiO_2 nanotube morphology. It was revealed that the nanotubes (NTs) diameter and thickness increase with increasing the applied potential while the variation of other parameters (composition of electrolyte and anodization temperature) have no influence on the diameter of the tubes. However, it was observed that the tube length increases with the increase of applied potential, anodization temperature, and time. In general, well-organized longer nanotubes with larger diameters are highly preferred for applications in a variety of fields.

It is well established that controlling the anodization parameters is the key to modifying the TNTs morphology and properties. However, examining all these parameters in detail requires consuming large amounts of raw materials and time. Moreover, each parameter does not act independently during the anodization process making it difficult to understand its distinct effect on the output. Response surface methodology (RSM) is one of the best available experimental designs that can be used to effectively investigate the effects of multiple independent variables and determine the optimal operating parameters [29–31]. Up to date, there is only a limited number of reported studies using the RSM technique for optimizing experiments of anodizing Ti alloys for different industrial applications and purposes [32–34]. Therefore, implementation of RSM is highly required for developing optimum anodization parameters that affect the morphology of TiO_2 nanotube arrays.

In this study, the RSM technique is employed for optimizing the anodizing parameters in order to achieve the desired morphology of TiO_2 nanotubes (TNTs). The investigated parameters are the electrolyte concentration (C), anodization voltage (V), and anodization time (t). Ethylene glycol (EG) with 2.5 vol% H_2O was utilized as an electrolyte by varying the concentration of ammonium fluoride (NH_4F). The TNT morphology and crystalline structure were monitored using Field Emission Scanning Electron Microscopy (FESEM) X-ray diffraction (XRD) analyses. This study provides new insights for producing highly efficient TiO_2 nanotubes (TNTs) with suitable morphology for possible applications in various environmental and energy fields.

2. Experimental procedures

2.1. Fabrication of TNTs

To fabricate TiO_2 nanotubes cost-effective and easily controllable electrochemical anodization method was employed in this study. Commercially available titanium (Ti) foil (purity 99.5%) of 0.2 mm thickness was purchased from Sigma-Aldrich company and cut into desired dimensions (25 mm × 20 mm) to utilize as a substrate during the anodization process. Prior to the experiment, Ti foils were cleaned ultrasonically using acetone (C_3H_6O), ethyl alcohol (C_2H_6O), and deionized water (DI) for 15 min, respectively. After ultrasonication, the specimens were etched in a solution comprising of HNO_3, HF, and DI water in a volume ratio of 1:1:3 for about 20 s, to clean the surface from impurities and remove the inherent oxide layer, finally rinsed with DI water and dried naturally in air. The anodization process was conducted under a direct power supply using a two-electrode reactor, with the Ti foil as anode and graphite as cathode maintaining a spacing of 2 cm between each electrode. Ethylene glycol (EG) based electrolyte has been used throughout the experiment taking ammonium fluoride (NH_4F) as a source of fluoride ion (F^-) with 2.5 vol% H_2O. The Pt-PTFE electrode holder has been employed to hold and place the electrodes inside the solution. The electrolyte solution was stirred for homogenous dissolution using a magnetic stirrer and kept at room temperature during the anodization process. The range of anodizing parameters is tabulated in Table 1. Herein, two-step anodization was followed. In the first step, anodization was carried out for 30 min, and then as-formed TNT layers were ultrasonically rinsed in the DI water for 10 min to remove the initial layer. The previous samples were used for the second step of anodization using identical conditions as the first step. Finally, the anodized samples were rinsed with DI water and dried in the atmosphere following annealing at 500 °C for 2 h prior to further analysis.

2.2. Analysis methods

The morphology of the TNT surface has been monitored by Field Emission Scanning Electron Microscopy (FESEM, JSM-7800 F), furnished with an energy dispersive X-ray spectroscopy (EDX) for elemental analysis. To capture pictures, a 5.0 kV accelerating voltage was applied. The identification of phase and crystal planes of the attained TiO_2 nanotubes was determined by X-ray diffraction (XRD) using a PANalytical brand and X'Pert^3 Powder model diffractometer (Cu anode, $\lambda = 0.15418$ nm) over the 2θ range (3–150°), with an Inorganic Crystal Structure Database (ICSD).

2.3. Design of experiments (DoE)

The anodizing parameters to form TiO_2 nanotubes were optimized using RSM in central composite design (CCD). CCD has been employed to study the effects of NH_4F concentrations (wt%), anodization voltage (V), and time (min.) on nanotubes diameter (nm) and length (nm). The

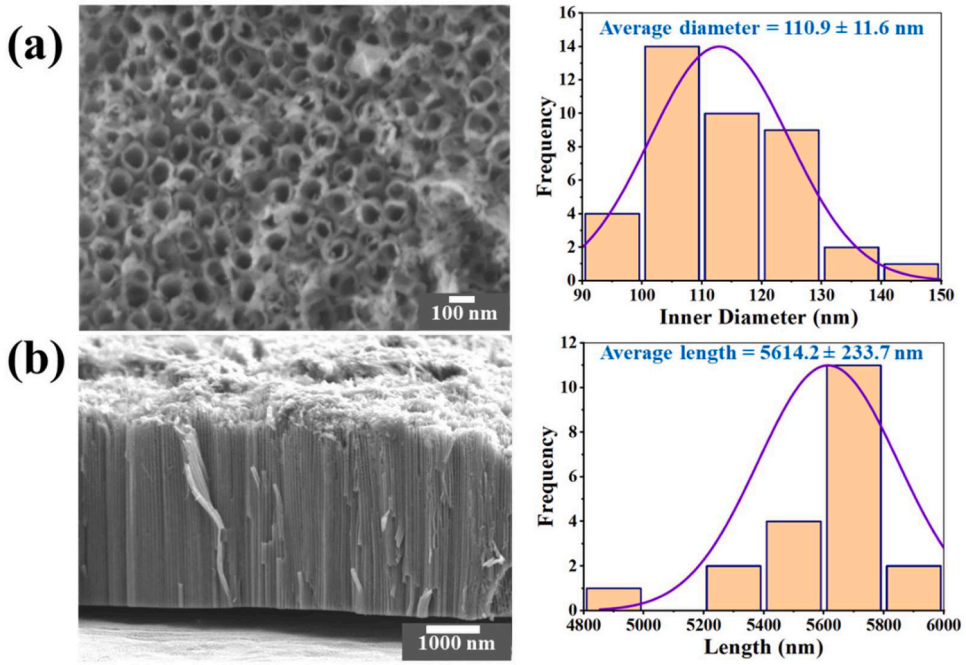

Fig. 1. FESEM images histogram diagram at central anodizing parameters (0.4 wt% NH_4F, 40 V and 120 min) (a) Top view and (b) Cross-sectional view.

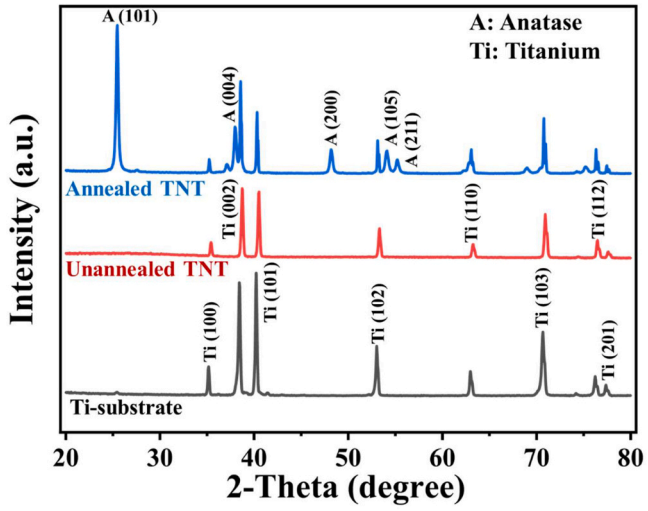

Fig. 2. XRD pattern of Ti-substrate, Unannealed TiO_2 nanotubes, and TiO_2 nanotubes annealed at 500 °C for 2 h.

variables were generated and examined using the Design Expert software (version SE360). Following Eq. (1), a total of 20 treatments were selected, including six (06) axial points, eight (08) factorial points, and six (06) central points. Where n_c (= 6) refers to the number of repetitions of treatment performed at the center and k (= 3) the number of treatment components. The actual and coded levels of variables are listed in Table 1.

$$N = 2^k + 2k + n_c \quad (1)$$

$$Z = \frac{(Z_0 - Z_c)}{\Delta Z} \quad (2)$$

$$Y = \beta_0 + \sum \beta_i X_i + \sum \beta_{ii} X_i^2 + \sum \beta_{ij} X_i X_j \quad (3)$$

Actual levels of independent variables were coded in accordance with Eq. (2), where Z and Z_0 represent actual and coded levels of independent variables, respectively. ΔZ stands for step change while Z_C denotes actual value at the central point. The experimental variables and response variables are summarized in Table 2. The mathematical association between the input variables and the resulting responses was developed by fitting the experimental data to a second-order polynomial as follows Eq. (3). Where Y stands for the response variable, β_o the constant, and β_i, β_{ii} and β_{ij} are the linear, quadratic and interactive coefficients respectively; X_i and X_j represent the independent variables. Moreover, the same software (Design Expert) was adopted for the multiple regression analysis and analysis of variance (ANOVA).

3. Results and discussion

3.1. Characteristics of anodized TNTs

To present the morphology of as-prepared TiO_2 nanotubes, a central combination of anodizing parameters was chosen (0.4 wt% NH_4F, 40 V, and 120 min). Fig. 1 displays the FESEM images of TNTs with a histogram diagram. The image exhibits open-mouth tube morphology with a tube opening of 110.9 ± 11.6 nm and a 5614.2 ± 233.7 nm tube length. The morphology attained in this study is consistent with the previous study conducted by Ribeiro and coworkers [35]. The XRD patterns of the anodized TNT samples (unannealed and annealed) and the unprocessed Ti substrate are demonstrated in Fig. 2. Ti metal peaks are the sole phase that may be seen in the XRD pattern of the Ti substrate. These peaks may also be seen in the XRD patterns of the unannealed TNTs, indicating that they are amorphous at this stage [36–38]. This amorphous phase is changed into the anatase phase by thermally treating it at 500 °C for two hours. The formation of the anatase phase is confirmed by the XRD analysis of the annealed samples (Fig. 2). The 2θ peaks at 25.3°, 37.7°, 48.0°, 53.7°, 55.0°, and 62.9° are attributed to the planes (101), (004), (200), (105), and (211) belong exclusively to the anatase phase [39,40].

3.2. Effect of independent variables on diameter of TNTs

The effect of electrolyte concentration (NH_4F, wt%), anodization voltage, and time were selected in order to examine the effects on nanotube diameter and length. To correlate the input variables and corresponding responses, a central composite design was utilized. In the

Table 3
ANOVA results of the response surface quadratic model for the diameter of TNTs.

Source	Sum of squares	DoF	Mean square	F-value	p-value	Comments
Model	22,161.91	9	2462.43	59.04	< 0.0001	Significant
X_1-NH_4F Conc.	4.06	1	4.06	0.0973	0.7615	
X_2-Voltage	1171.81	1	1171.81	28.09	0.0003	
X_3-Time	1793.18	1	1793.18	42.99	< 0.0001	
X_1X_2	7.60	1	7.60	0.1823	0.6784	
X_1X_3	4.20	1	4.20	0.1008	0.7574	
X_2X_3	3469.44	1	3469.44	83.18	< 0.0001	
X_1^2	739.49	1	739.49	17.73	0.0018	
X_2^2	12,653.61	1	12,653.61	303.37	< 0.0001	
X_3^2	4230.55	1	4230.55	101.43	< 0.0001	
Residual	417.10	10	41.71			
Lack of Fit	381.24	5	76.25	10.63	0.107	Not Significant
Pure Error	35.86	5	7.17			
Cor Total	22,579.01	19				

Note: $p < 0.01$ highly significant; $0.01 < p < 0.05$ significant; $p > 0.05$ not significant.

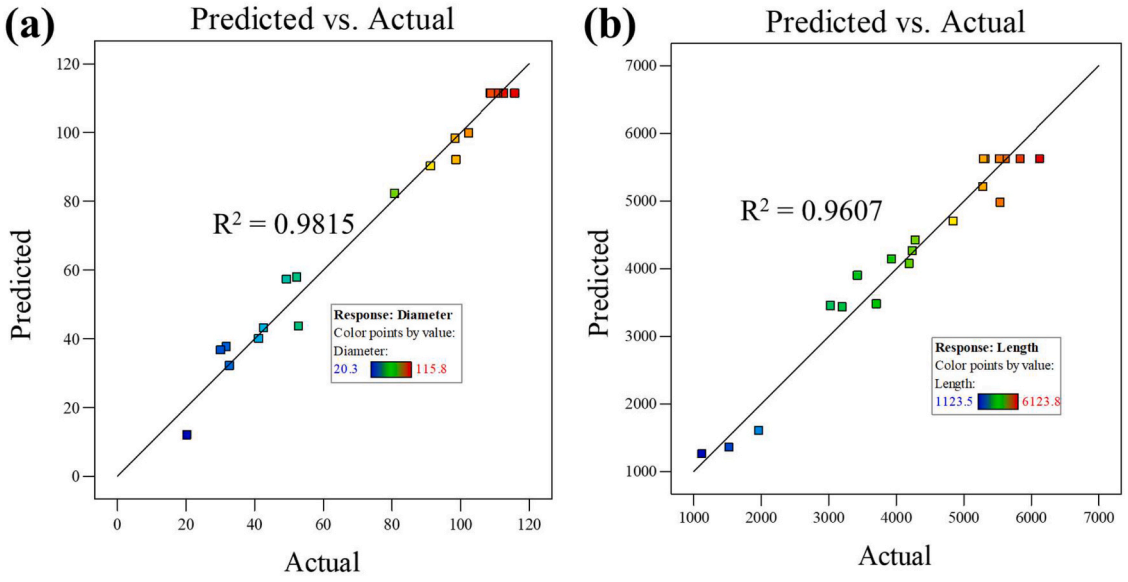

Fig. 3. Correlation between predicted and actual values of response for (a) nanotubes diameter and (b) nanotubes length.

Table 4
Evaluated regression coefficient values, standard error and 95% CI for the final regression model of the nanotube diameter (D).

Factor	Coefficients (Coded factors)	Standard error	95% CI Low	95% CI High
Intercept (β_0)	+111.42	2.63	105.55	117.29
X_1-NH_4F Conc. (β_1)	-0.5452	1.75	-4.44	3.35
X_2-Voltage (β_2)	+9.26	1.75	5.37	13.16
X_3-Time (β_3)	-11.46	1.75	-15.35	-7.56
X_1X_2 (β_{12})	-0.9750	2.28	-6.06	4.11
X_1X_3 (β13)	-0.7250	2.28	-5.81	4.36
X_2X_3 (β_{23})	-20.82	2.28	-25.91	-15.74
X_1^2 (β_{11})	-7.16	1.70	-10.95	-3.37
X_2^2 (β_{22})	-29.63	1.70	-33.42	-25.84
X_3^2 (β_{33})	-17.13	1.70	-20.92	-13.34
Adjusted R^2	0.9649			
Predicted R^2	0.8666			
Adequate Precision	21.76			

present study, 20 optimal runs were suggested by DoE, involving the fewest number of experiments possible for each combination of independent variables. The collected data were analyzed using the ANOVA analysis at a confidence level of 95%. The outcomes achieved by ANOVA for the dependent variable nanotubes diameter, are mentioned in Table 3. The analysis of ANOVA recommended a quadratic polynomial model to fit the experimental data with nanotube diameter. The value of F appeared to be 59.04 from the analysis, and the generated model's lowered p-value (< 0.0001) confirms the validity and accuracy of the model. The F value in statistics is the variance of the group means, whereas the p-value is a probability. Higher F-values and lower p-values signify a very significant impact on the response variable [31,41]. It is evident from the ANOVA table, that the variables X_1, X_1X_2, and X_1X_3 have no significant influence on the model. Non-significant lack of fit ($p \leq 0.05$) for all examined variables also signifies the precision of the statistical model [42,43]. Closer to the unity coefficient of determination (R^2) value indicates a better fitting of the model to actual data and predicted data [29,31,44]. In the present study, the R^2 value of 0.9815 for responses of nanotube diameter illustrates that the effect of actual values on predicted values could be described adequately using a quadratic model (Fig. 3a).

The regression analysis is one of the well-known approaches to compare the proposed model with the anticipated responses [45,46]. To fit the response function of nanotube diameter on independent variables, regression analysis was carried out. The regression coefficients along with standard error and 95% CI for the final regression model of the nanotube diameter are presented in Table 4. The coefficients of the proposed model are estimated by the least squares method. The final

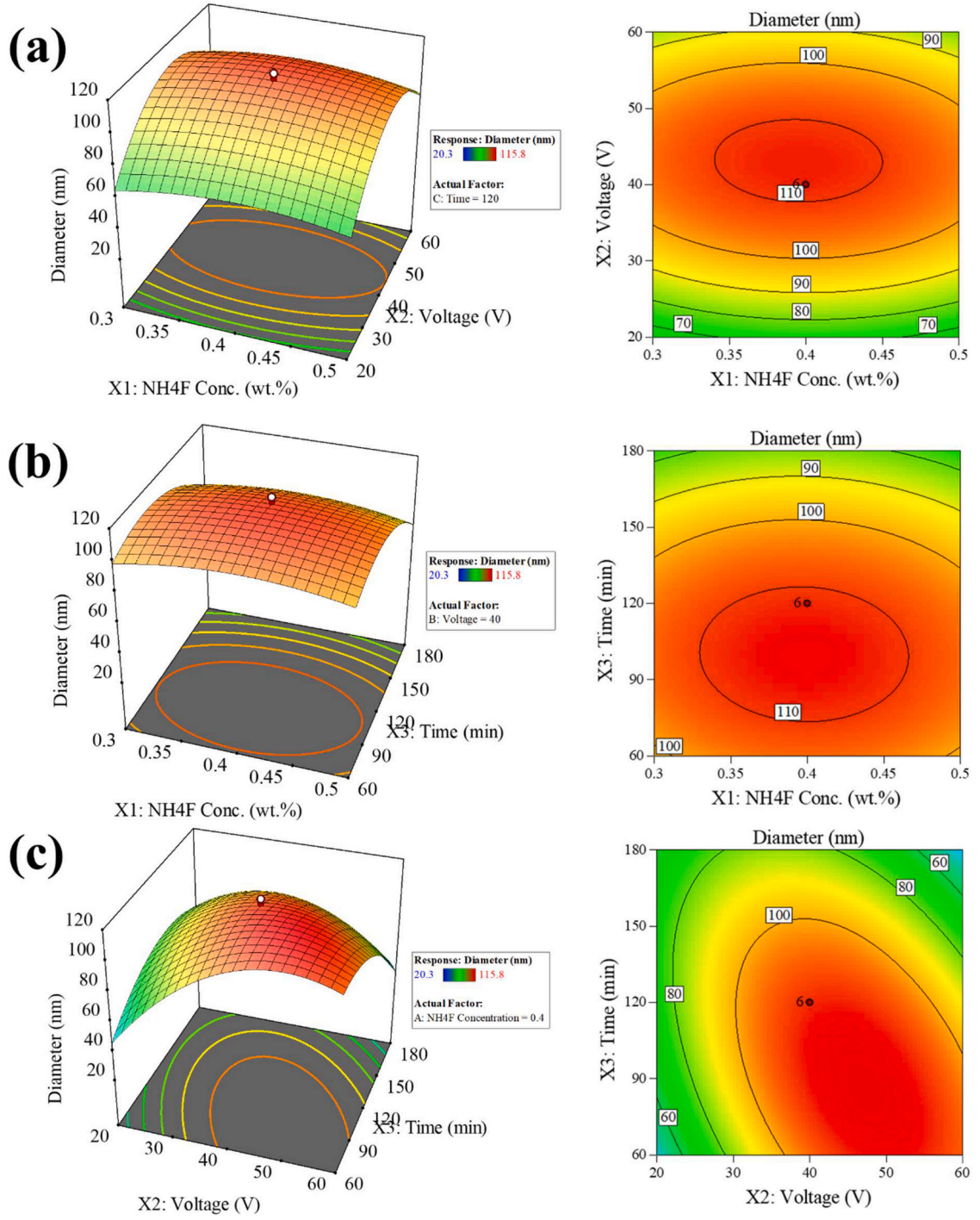

Fig. 4. 3D surface plot and its corresponding contour plot displaying the interactions between the variables affecting the diameter of the nanotubes: (a) NH_4F concentration and anodization voltage (keeping anodization time constant), (b) NH_4F concentration and anodization time (keeping anodization voltage constant), and (c) anodization voltage and time (keeping NH_4F concentration constant).

empirical models for nanotubes diameter (nm) in terms of coded factors after excluding insignificant terms is given in Eq. (4). The multiple regression coefficient for Eq. (4) (adj. $R^2 = 0.9649$) was found to be higher than 0.80, indicating that only 3.51% of the total variation for nanotubes diameter cannot be explained by the proposed regression model. The pred. R^2 of 0.8666 is in reasonable agreement with the adj. R^2 of 0.9649; i.e., the difference is less than 0.2. The importance of the model is demonstrated by the close proximity between the coefficient of determination ($R^2 = 0.9815$) and the adjusted coefficient of determination (adj. $R^2 = 0.9649$) in the present investigation. Signal to noise ratio (adeq. precision) of 21.76 (>> 4), indicated that the model has a strong enough signal to be used for optimization.

$$\text{Nanotubes Diameter (D)} = +111.42 + 9.26 * X_2 - 11.46 * X_3 - 20.82 * X_2X_3 - 7.16 * X_1^2 - 29.63 * X_2^2 - 17.13 * X_3^2 \quad (4)$$

To demonstrate the combined effects of the factors on the responses, response surface plots have been developed for the fitted model as a function of two independent variables while keeping the third variable constant. Fig. 4 presents the 3D surface plot and its corresponding contour plot displaying the interactions between the independent

Table 5
ANOVA results of the response surface quadratic model for length of TNTs.

Source	Sum of squares	DoF	Mean square	F-value	p-value	Comments
Model	3.930E+07	9	4.367E+06	27.14	< 0.0001	Significant
X_1-NH_4F Conc.	44,589.43	1	44,589.43	0.2771	0.6101	
X_2-Voltage	5.932E+06	1	5.932E+06	36.86	0.0001	
X_3-Time	1.409E+06	1	1.409E+06	8.76	0.0143	
X_1X_2	33,995.28	1	33,995.28	0.2113	0.6556	
X_1X_3	1.383E+05	1	1.383E+05	0.8592	0.3758	
X_2X_3	9.298E+06	1	9.298E+06	57.78	< 0.0001	
X_1^2	3.805E+06	1	3.805E+06	23.65	0.0007	
X_2^2	1.906E+07	1	1.906E+07	118.47	< 0.0001	
X_3^2	2.528E+06	1	2.528E+06	15.71	0.0027	
Residual	1.609E+06	10	1.609E+05			
Lack of Fit	1.103E+06	5	2.205E+05	2.18	0.2067	Not significant
Pure Error	5.066E+05	5	1.013E+05			
Cor Total	4.091E+07	19				

$p < 0.01$ highly significant; $0.01 < p < 0.05$ significant; $p > 0.05$ not significant.

Table 6
Evaluated regression coefficient values, standard error and 95% CI for the final regression model of the nanotube length (L).

Factor	Coefficients (Coded factors)	Standard error	95% CI Low	95% CI High
Intercept (β_0)	+5622.48	163.61	5257.94	5987.03
X_1-NH_4F Conc. (β_1)	-57.14	108.55	-299.01	184.73
X_2-Voltage (β_2)	+659.08	108.55	417.21	900.95
X_3-Time (β_3)	+321.20	108.55	79.33	563.06
X_1X_2 (β_{12})	-65.19	141.83	-381.20	250.82
X_1X_3 (β13)	+131.46	141.83	-184.55	447.47
X_2X_3 (β_{23})	-1078.06	141.83	-1394.07	-762.05
X_1^2 (β_{11})	-513.87	105.67	-749.32	-278.42
X_2^2 (β_{22})	-1150.18	105.67	-1385.63	-914.73
X_3^2 (β_{33})	-418.87	105.67	-654.32	-183.42
Adjusted R^2	0.9253			
Predicted R^2	0.7761			
Adequate Precision	15.3765			

variables affecting the nanotube diameter. The interactive effects of NH_4F concentration and anodization voltage at a fixed anodization time of 120 min can be seen in Fig. 4(a). It is evident from Fig. 4(a) that the nanotube diameter increases slightly with an increase in the NH_4F concentration up to 0.4 wt% and then goes on decreasing with a further increase in NH_4F concentration beyond 0.4 wt%. Consequently, the diameter of the nanotubes increases continuously with an increase in the anodization voltage and reaches the highest value of about 115.8 nm at a voltage of 45.4 V. This is consistent with the study conducted by Kawamura et al. [47]. After reaching the diameter optimum level then goes on decreasing gradually with a further increase in voltage beyond 45.4 V. A possible explanation for this effect is that at elevated concentrations of NH_4F, the formation of closely packed inhomogeneous nanotubular structures increased, thereby facilitating the reduction of the NT diameter [25,48,49]. At elevated voltage (above 50 V) tube length starts to collapse with a less uniform mouth top edge which leads to the reduction in NTs diameter [50], as shown in Figs. S1–S3. The interaction effects of anodization time and NH_4F concentration on the diameter of NTs are depicted in Fig. 4(b) while keeping a constant anodization voltage of 40 V. It can be observed that a similar trend of NT diameter is followed in Fig. 4(a) due to the changes in NH_4F concentration. Overall, the concentration of NH_4F does not have a substantial effect on the average diameter of the NTs; however, the homogeneity of the structure greatly breaks up, remarkably the wall structure. The nanotube diameter increases steadily with an increase in the anodization time. Fig. 4(c) shows the 3D response surface and contour plot of the combined effect of anodization voltage and time on NTs diameter with the concentration of NH_4F being fixed at zero level (NH_4F conc. = 0.4 wt %). It can be revealed from the plot that both variables have a great effect on the diameter of NTs. As can be seen from the figure, the diameter of the NTs increases with the increase in voltage and time and reaches the maximum value of 115.8 nm near the highest values of both variables. Initially, there was a sharp increasing trend of diameter for both variables, which slightly tended to decrease after voltage 50 V and 150 min anodization time. This may be due to the collapse of tubular structures at elevated voltage and the formation of the nanograss at a longer anodization time [25,35], please refer to Fig. S3.

3.3. Effect of independent variables on length of TNTs

Table 5 summarizes the results of the ANOVA for the response of TiO_2NTs length. The model's F-value of 27.14 and p-value of less than 0.0001 imply the significance of the suggested quadratic model. Similar to the response of NTs diameter, the variables X_1, X_1X_2, and X_1X_3 have insignificant influence on the model of NTs length. Non-significant lack of fit test also supports the accuracy of the model. Fig. 3(b) also shows a strong correlation ($R^2 = 0.9607$) with actual versus predicted variables. These outcomes demonstrated that the model fitted the data accurately. The F-value and p-value were used to find regression coefficients, standard error, and significance of each coefficient, as presented in Table 6. The length of the NTs can be predicted using the resulting reduced quadratic polynomial Eq. (5).

$$\text{Nanotubes Length (L)} = +5622.48 + 659.08 * X_2 + 321.20 * X_3 - 1078.06 * X_2X_3 - 513.87 * X_1^2 - 1150.18 * X_2^2 - 418.87 * X_3^2 \quad (5)$$

The interactive effects of independent variables namely concentration of NH_4F, anodization voltage, and time on the mean length of NTs are depicted in Fig. 5. Fig. 5(a) shows the combined effect of NH_4F concentration and voltage on the length of NTs being fixed at zero level (t = 120 min). Both parameters have a quadratic effect on the length of nanotubes. At a certain level of NH_4F concentration and voltage, the length of NTs increases and after reaching an optimum highest length of 6123.8 nm starts to reduce. The changes in NT length with the variation of NH_4F concentration are not apparent compared to voltage. After reaching a length of NTs up to 6123.8 nm at voltage 45.2 V, the length reaches 3027.2 nm at 60 V due to the fast increase in the electrolyte temperature, which initiates the breakdown event [51]. Fig. 5(b) represents the interactive effect of NH_4F concentration and anodization time on the mean length of NTs. Similar to Fig. 5(a), the effect of both parameters is quadratic. The most notable interaction was found between anodization voltage and time for the response of NTs length at 0.4 wt% NH_4F concentration (Fig. 5c). When anodization is subjected to a higher voltage for a longer time, the tube mouth leads to the break-up of larger lengths into smaller ones [50], as illustrated in Fig. S3. The lengths of the tubes stay the same when an electrochemical equilibrium

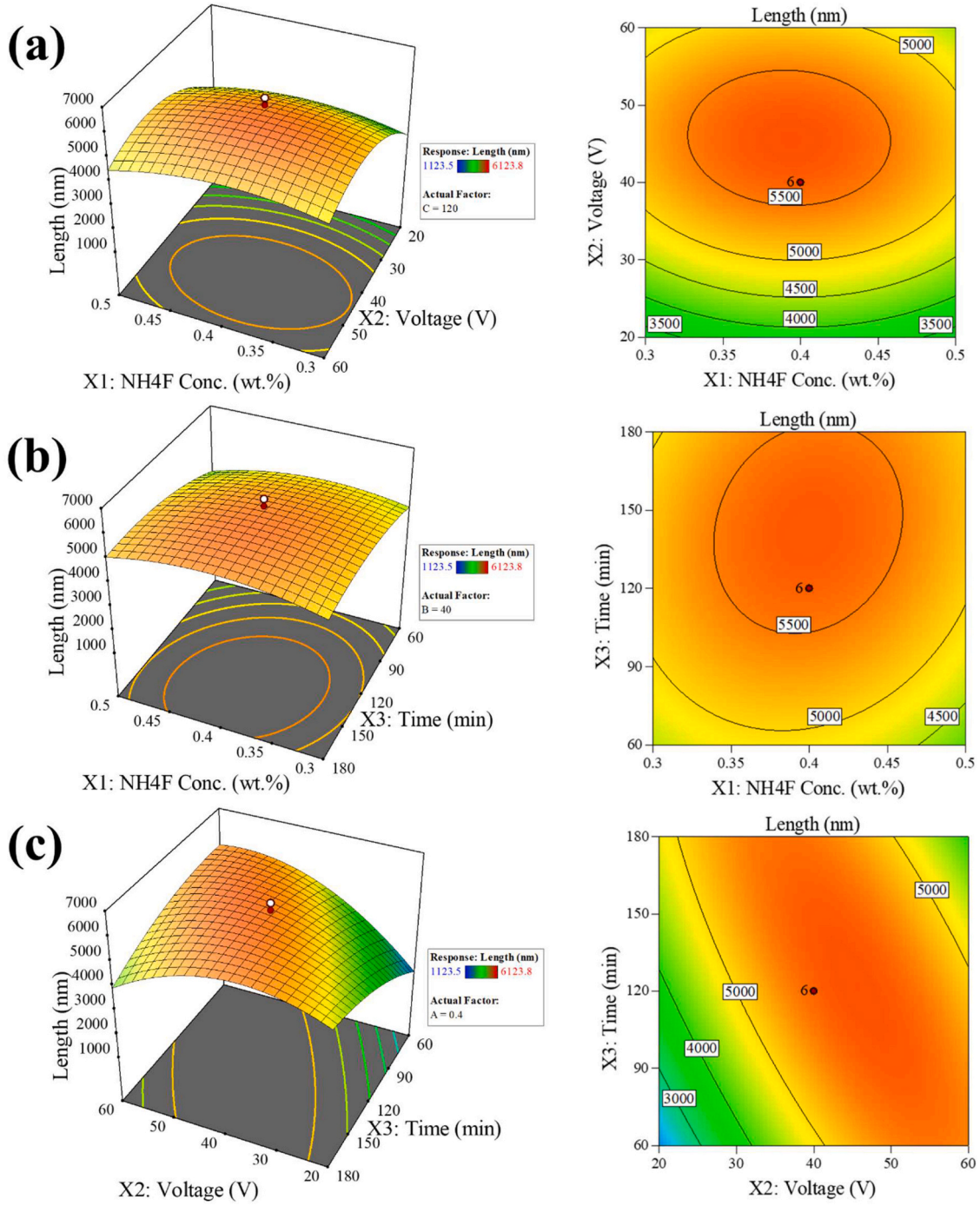

Fig. 5. 3D surface plot and its corresponding contour plot displaying the interactions between the variables affecting the length of the nanotubes: (a) NH_4F concentration and anodization voltage (keeping anodization time constant), (b) NH_4F concentration and anodization time (keeping anodization voltage constant) and (c) anodization voltage and time (keeping NH_4F concentration constant).

Table 7
Predicted and experimental response at optimized conditions.

Optimum conditions	**Coded levels**	**Actual levels**	**Desirability**
NH_4F conc. (wt%)	- 1.00	0.31	
Voltage (V)	- 0.08	38.44	0.82
Time (min.)	- 0.85	69.37	
Response	**Predicted**	**Experimental**	
Diameter (nm)	99.31	90.57 ± 13.85	
Length (nm)	4572.64	4686.68 ± 381.92	

is reached between chemical dissolution and electrochemical etching of TiO_2 [52,53]. Chemical etching occurs on the top walls of the tubes during a prolonged anodizing process, giving the upper morphology a nanograss aspect [54]. TiO_2 NTs bend and collapse at greater rates with longer anodization times, which results in a nanograss-like appearance [54,55]. The appearance of this structure thus signifies the completion of the anodization process.

3.4. Optimized anodizing conditions

The desirability function has been utilized for identifying the

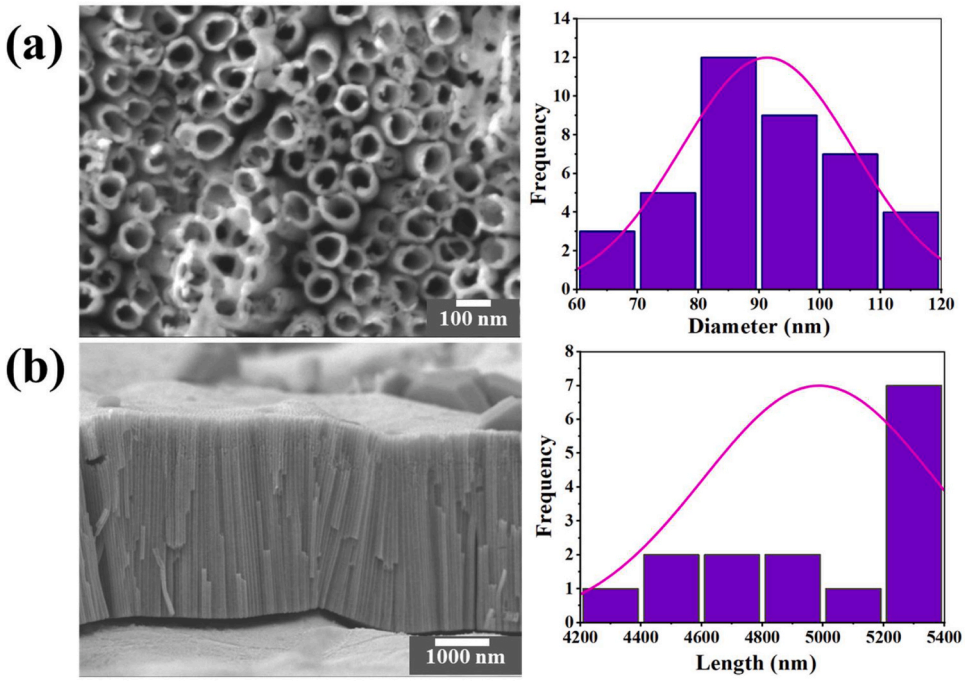

Fig. 6. TiO_2 nanotube morphology at optimized anodizing parameters (a) Top view and (b) Cross-sectional view.

optimum conditions. The factor settings that have the highest overall desirability are selected as the optimum conditions [56,57]. Desirable goals for optimization of nanotube morphology were set up with a minimum concentration of NH_4F, anodization voltage, and time to achieve maximum diameter and length of NTs. The optimum concentration of NH_4F, anodization voltage, and time were obtained at 0.31 (wt %), 38.44 V, and 69.37 min respectively at 0.82 desirability. The desirability value close to unity indicates a good prediction of the optimized model [58]. The optimum parameters revealed through RSM were subsequently verified by performing the experiment under optimum anodizing conditions. In order to verify the predicted morphology of NTs, the anodization was carried out in three replications utilizing the optimum anodizing parameters. At optimum anodizing conditions, predicted response values for nanotube diameter and length were 99.31 and 4572.64 nm, while the experimental values were found 90.57 $\pm$ 13.85 and 4686.68 $\pm$ 381.92 nm, respectively (Table 7). It has been observed that the experimental results were found to be in fairly good conformity with predicted values. Well-organized and vertically aligned tubes with uniform diameters were obtained at optimized anodizing parameters as illustrated in Fig. 6. It is worth mentioning that the optimized values of fluoride concentration, potential, and time are only valid for the composition of the electrolyte used in the present study. As soon as the water content changes, or another electrolyte base (glycerol, diethylene glycol, DMSO, water) is chosen, the values may change.

4. Conclusions

The present study was conducted to optimize anodizing parameters for getting the desired morphology of TiO_2 nanotubes using the central composite design of RSM. ANOVA analysis suggested a quadratic polynomial model to be suitable for predicting responses namely nanotubes diameter and length. The optimum anodizing parameters for the production of nanotubes with higher diameter and longer length have been identified to be 0.31 wt% NH_4F concentration, 38.44 V applied potential, and 69.37 min of anodization time. At optimized anodizing settings, well-organized, vertically aligned tubes with uniform diameters were produced. It was observed that the experimental values for the diameter and length of NTs were in good agreement with model-predicted values with relatively small standard error. Good prediction of the optimized model is indicated by the desirability value being near unity.

CRediT authorship contribution statement

Md. Arif Hossen: Conceptualization, Data curation, Formal analysis, Investigation, Methodology, Software, Validation, Visualization, Writing – original draft. **Azrina Abd Aziz:** Supervision, Writing – review & editing. **Riyadh Ramadhan Ikreedeegh:** Writing – original draft, Writing – review & editing. **Aamina Din Muhammad:** Investigation, Methodology. **Nurashikin Yaacof:** Writing – review & editing. **Kah Hon Leong:** Writing – review & editing. **Lihua Wu:** Funding acquisition.

Declaration of Competing Interest

The authors declare that they have no known competing financial interests or personal relationships that could have appeared to influence the work reported in this paper.

Data availability

Data can be available by contacting the corresponding author.

Acknowledgment

The authors are gratified to acknowledge the help and support provided by the Universiti Malaysia Pahang Al-Sultan Abdullah (UMPSA) internal Product Development Unit Grant (PDU 213221).

Appendix A. Supporting information

Supplementary data associated with this article can be found in the online version at doi:10.1016/j.nxmate.2023.100061.

References

[1] M. Assefpour-Dezfuly, C. Vlachos, E.H. Andrews, Oxide morphology and adhesive bonding on titanium surfaces, J. Mater. Sci. 19 (1984) 3626–3639.

[2] K. Dai, J. Lv, J. Zhang, G. Zhu, L. Geng, C. Liang, Efficient visible-light-driven splitting of water into hydrogen over surface-fluorinated anatase TiO2 nanosheets with exposed {001} facets/layered CdS–diethylenetriamine nanobelts, ACS Sustain. Chem. Eng. 6 (10) (2018) 12817–12826.
[3] D. Adekoya, M. Tahir, N.A.S. Amin, Recent trends in photocatalytic materials for reduction of carbon dioxide to methanol, Renew. Sustain. Energy Rev. 116 (2019), 109389.
[4] R.R. Ikreedeegh, M. Tahir, A critical review in recent developments of metal-organic-frameworks (MOFs) with band engineering alteration for photocatalytic CO_2 reduction to solar fuels, J. CO_2 Util. 43 (2021), 101381.
[5] M.A. Hossen, H.M. Solayman, K.H. Leong, L.C. Sim, Y. Nurashikin, A. Abd Aziz, M. U. Monir, Recent progress in TiO2-Based photocatalysts for conversion of CO_2 to hydrocarbon fuels: a systematic review, Results Eng. (2022), 100795.
[6] C.B. Anucha, I. Altin, E. Bacaksiz, V.N. Stathopoulos, Titanium dioxide (TiO_2)-based photocatalyst materials activity enhancement for contaminants of emerging concern (CECs) degradation: in the light of modification strategies, Chem. Eng. J. Adv. 10 (2022), 100262.
[7] Y. Zhao, N. Hoivik, K. Wang, Recent advance on engineering titanium dioxide nanotubes for photochemical and photoelectrochemical water splitting, Nano Energy 30 (2016) 728–744.
[8] B. Çakıroğlu, M. Özacar, Efficient chemiluminescence harnessing via slow photons in sensitized TiO2 nanotubes for the photoelectrochemical biosensing, J. Electroanal. Chem. 878 (2020), 114676.
[9] M.A. Hossen, H.M. Solayman, K.H. Leong, L.C. Sim, N. Yaacof, A. Abd Aziz, M. U. Monir, A comprehensive review on advances in TiO2 nanotube (TNT)-based photocatalytic CO_2 reduction to value-added products, Energies 15 (22) (2022) 8751.
[10] F. Khatun, A. Abd Aziz, L.C. Sim, M.U. Monir, Plasmonic enhanced Au decorated TiO2 nanotube arrays as a visible light active catalyst towards photocatalytic CO_2 conversion to CH4, J. Environ. Chem. Eng. 7 (6) (2019), 103233.
[11] L.C. Sim, K.S. Koh, K.H. Leong, Y.H. Chin, A. Abd Aziz, P. Saravanan, In situ growth of g-C3N4 on TiO2 nanotube arrays: construction of heterostructures for improved photocatalysis properties, J. Environ. Chem. Eng. 8 (1) (2020), 103611.
[12] R.R. Ikreedeegh, M. Tahir, Photocatalytic CO_2 reduction to CO and CH 4 using gC3N4/RGO on titania nanotube arrays (TNTAs), J. Mater. Sci. 56 (2021) 18989–19014.
[13] M.A. Hossen, F. Khatun, R.R. Ikreedeegh, A.D. Muhammad, A. Abd Aziz, K. H. Leong, M.U. Monir, Enhanced photocatalytic CO_2 reduction to CH4 using novel ternary photocatalyst RGO/Au-TNTAs, Energies 16 (14) (2023) 5404.
[14] I. Kim, W.Y. Choi, Hybrid gas sensor having TiO2 nanotube arrays and SnO2 nanoparticles, Int. J. Nanotechnol. 14 (1–6) (2017) 155–165.
[15] X. Tong, W. Shen, X. Zhang, J.P. Corriou, H. Xi, Synthesis and density functional theory study of free-standing Fe-doped TiO2 nanotube array film for H2S gas sensing properties at low temperature, J. Alloy. Compd. 832 (2020), 155015.
[16] Z. Yi, Y. Zeng, H. Wu, X. Chen, Y. Fan, H. Yang, P. Wu, Synthesis, surface properties, crystal structure and dye-sensitized solar cell performance of TiO2 nanotube arrays anodized under different parameters, Results Phys. 15 (2019), 102609.
[17] D. Luo, B. Liu, A. Fujishima, K. Nakata, TiO2 nanotube arrays formed on Ti meshes with periodically arranged holes for flexible dye-sensitized solar cells, ACS Appl. Nano Mater. 2 (6) (2019) 3943–3950.
[18] Z. Peng, J. Ni, Surface properties and bioactivity of TiO2 nanotube array prepared by two-step anodic oxidation for biomedical applications, R. Soc. Open Sci. 6 (4) (2019), 181948.
[19] A. Bandyopadhyay, A. Shivaram, I. Mitra, S. Bose, Electrically polarized TiO2 nanotubes on Ti implants to enhance early-stage osseointegration, Acta Biomater. 96 (2019) 686–693.
[20] V. Sivaprakash, L. Natrayan, R. Suryanarayanan, R. Narayanan, P. Paramasivam, Electrochemical anodic synthesis and analysis of TiO2 nanotubes for biomedical applications, J. Nanomater. 2021 (2021) 1–10.
[21] M.Z. Ge, C.Y. Cao, J.Y. Huang, S.H. Li, S.N. Zhang, S. Deng, Y.K. Lai, Synthesis, modification, and photo/photoelectrocatalytic degradation applications of TiO2 nanotube arrays: a review, Nanotechnol. Rev. 5 (1) (2016) 75–112.
[22] V. Galstyan, J.M. Macak, T. Djenizian, Anodic TiO2 nanotubes: a promising material for energy conversion and storage, Appl. Mater. Today 29 (2022), 101613.
[23] M.A. Hossen, N. Yaacof, A. Abd Aziz, W. Lihua, Latest progress on the influencing factors affecting the formation of TiO2 nanotubes (TNTs) in electrochemical anodization- a minireview, Acta Chem. Malays. 7 (1) (2023) 08–15.
[24] S. Ozkan, A. Mazare, P. Schmuki, Critical parameters and factors in the formation of spaced TiO2 nanotubes by self-organizing anodization, Electrochim. Acta 268 (2018) 435–447.
[25] A.B. Tesler, M. Altomare, P. Schmuki, Morphology and optical properties of highly ordered TiO2 nanotubes grown in NH4F/o-H3PO4 electrolytes in view of light-harvesting and catalytic applications, ACS Appl. Nano Mater. 3 (11) (2020) 10646–10658.
[26] H.E. Prakasam, K. Shankar, M. Paulose, O.K. Varghese, C.A. Grimes, A new benchmark for TiO2 nanotube array growth by anodization, J. Phys. Chem. C 111 (20) (2007) 7235–7241.
[27] J.M. Macak, H. Hildebrand, U. Marten-Jahns, P. Schmuki, Mechanistic aspects and growth of large diameter self-organized TiO2 nanotubes, J. Electroanal. Chem. 621 (2) (2008) 254–266.
[28] S. Ozkan, N.T. Nguyen, A. Mazare, R. Hahn, I. Cerri, P. Schmuki, Fast growth of TiO2 nanotube arrays with controlled tube spacing based on a self-ordering process at two different scales, Electrochem. Commun. 77 (2017) 98–102.
[29] T. Mehmood, A. Ahmed, A. Ahmad, M.S. Ahmad, M.A. Sandhu, Optimization of mixed surfactants-based β-carotene nanoemulsions using response surface methodology: an ultrasonic homogenization approach, Food Chem. 253 (2018) 179–184.
[30] Y. Zheng, J. Wang, C. Liu, Y. Lu, X. Lin, W. Li, Z. Zheng, Optimizing Ni–Ce/HZSM-5 catalysts for ex-situ conversion of pine wood pyrolytic vapours into light aromatics and phenolic compounds, Int. J. Hydrog. Energy 45 (29) (2020) 14728–14743.
[31] N. Dutta, P. Mondal, A. Gupta, Optimization of process parameters using response surface methodology for maximum liquid yield during thermal pyrolysis of blend of virgin and waste high-density polyethylene, J. Mater. Cycles Waste Manag. 24 (3) (2022) 1182–1193.
[32] Z. Endut, M. Hamdi, W.J. Basirun, Optimization and functionalization of anodized titania nanotubes for redox supercapacitor, Thin Solid Films 549 (2013) 306–312.
[33] S. Khameneh Asl, B. Mohammadi, A. Khataee, Optimization of anodizing parameters on photo decolorization of textile dye solution using N-doped titanium nanotubes with response surface methodology, Chem. Methodol. 4 (3) (2020) 258–275.
[34] N. Allal, A. Bourahla, F. Benharcha, A. Abdi, Z.B.D. Sayah, M. Trari, Anodizing parameters optimization of Ti–6Al–4V titanium alloy using response surface methodology, J. Indian Chem. Soc. 99 (6) (2022), 100470.
[35] B. Ribeiro, R. Offoiach, S. Rossetti, E. Salatin, M. Lekka, L. Fedrizzi, On growth and morphology of TiO2 nanotubes on CP-Ti by anodic oxidation in ethylene glycol electrolyte: influence of electrolyte aging and anodization parameters, Materials 15 (9) (2022) 3338.
[36] S.P. Albu, A. Ghicov, S. Aldabergenova, P. Drechsel, D. LeClere, G.E. Thompson, P. Schmuki, Formation of double-walled TiO2 nanotubes and robust anatase membranes, Adv. Mater. 20 (21) (2008) 4135–4139.
[37] B. Munirathinam, H. Pydimukkala, N. Ramaswamy, L. Neelakantan, Influence of crystallite size and surface morphology on electrochemical properties of annealed TiO2 nanotubes, Appl. Surf. Sci. 355 (2015) 1245–1253.
[38] E. Montakhab, F. Rashchi, S. Sheibani, Modification and photocatalytic activity of open channel TiO2 nanotubes array synthesized by anodization process, Appl. Surf. Sci. 534 (2020), 147581.
[39] K.M. Chahrour, F.K. Yam, A.M. Eid, Water-splitting properties of bi-phased TiO2 nanotube arrays subjected to high-temperature annealing, Ceram. Int. 46 (13) (2020) 21471–21481.
[40] A. Talla, N.J. Suliali, W.E. Goosen, Z.N. Urgessa, S.V. Motloung, J.R. Botha, Effect of annealing temperature and atmosphere on the structural, morphological and luminescent properties of TiO2 nanotubes, Phys. B Condens. Matter 640 (2022), 414026.
[41] N. Mansouriieh, M.R. Sohrabi, M. Khosravi, Optimization of profenofos organophosphorus pesticide degradation by zero-valent bimetallic nanoparticles using response surface methodology, Arab. J. Chem. 12 (8) (2019) 2524–2532.
[42] E.A. Alenyorege, H. Ma, J.H. Aheto, I. Ayim, F. Chikari, R. Osae, C. Zhou, Response surface methodology centred optimization of mono-frequency ultrasound reduction of bacteria in fresh-cut Chinese cabbage and its effect on quality, LWT 122 (2020), 108991.
[43] A. Sharma, D.S. Sogi, Optimization of enzyme aided pigment extraction from pumpkin (Cucurbita maxima Duch) using response surface methodology, J. Food Meas. Charact. 16 (2) (2022) 1184–1194.
[44] H. Ouachtak, A. El Guerdaoui, R. El Haouti, R. Haounati, H. Ighnih, Y. Toubi, M. L. Taha, Combined molecular dynamics simulations and experimental studies of the removal of cationic dyes on the eco-friendly adsorbent of activated carbon decorated montmorillonite Mt@ AC, RSC Adv. 13 (8) (2023) 5027–5044.
[45] K. Intani, S. Latif, A.R. Kabir, J. Müller, Effect of self-purging pyrolysis on yield of biochar from maize cobs, husks and leaves, Bioresour. Technol. 218 (2016) 541–551.
[46] M.T.H. Siddiqui, S. Nizamuddin, N.M. Mubarak, K. Shirin, M. Aijaz, M. Hussain, H. A. Baloch, Characterization and process optimization of biochar produced using novel biomass, waste pomegranate peel: a response surface methodology approach, Waste Biomass Valoriz. 10 (2019) 521–532.
[47] G. Kawamura, H. Ohmi, W.K. Tan, Z. Lockman, H. Muto, A. Matsuda, Ag nanoparticle-deposited TiO2 nanotube arrays for electrodes of Dye-sensitized solar cells, Nanoscale Res. Lett. 10 (2015) 1–6.
[48] C. Li, Y. Ni, J. Gong, Y. Song, T. Gong, X. Zhu, A review: research progress on the formation mechanism of porous anodic oxides, Nanoscale Adv. 4 (2) (2022) 322–333.
[49] C. Li, K. Luo, B. Yan, W. Sun, L. Jiang, P. Li, Y. Song, Simulation of anodic current and optimization of the fitting equation and the fitting algorithm during constant voltage anodization, J. Phys. Chem. C (2023).
[50] A.N. Dwojak, M.L. Vera, H.D. Traid, M.F. Maydana, M.I. Litter, C.E. Schvezov, Influence of anodizing variables on Cr (VI) photocatalytic reduction using TiO2 nanotubes obtained by anodic oxidation, Environ. Nanotechnol. Monit. Manag. 16 (2021), 100537.
[51] M. Alijani, H. Sopha, S. Ng, J.M. Macak, High aspect ratio TiO2 nanotube layers obtained in a very short anodization time, Electrochim. Acta 376 (2021), 138080.
[52] D. Khudhair, H.A. Hamedani, J. Gaburro, S. Shafei, S. Nahavandi, H. Garmestani, A. Bhatti, Enhancement of electro-chemical properties of TiO2 nanotubes for biological interfacing, Mater. Sci. Eng. C 77 (2017) 111–120.
[53] M.L. Puga, J. Venturini, C.S. ten Caten, C.P. Bergmann, Influencing parameters in the electrochemical anodization of TiO2 nanotubes: systematic review and meta-analysis, Ceram. Int. (2022).
[54] H. Fraoucene, D. Hatem, F. Vacandio, M. Pasquinelli, TiO2 nanotubes with nanograss structure: The effect of the anodizing voltage on the formation mechanism and structure properties, J. Electron. Mater. 48 (2019) 2046–2054.

[55] D. Regonini, C.R. Bowen, A. Jaroenworaluck, R. Stevens, A review of growth mechanism, structure and crystallinity of anodized TiO2 nanotubes, Mater. Sci. Eng. R Rep. 74 (12) (2013) 377–406.

[56] M. Manohar, J. Joseph, T. Selvaraj, D. Sivakumar, Application of desirability-function and RSM to optimise the multi-objectives while turning Inconel 718 using coated carbide tools, Int. J. Manuf. Technol. Manag. 27 (4–6) (2013) 218–237.

[57] A.I. Jabbr, H. Gaja, U.O. Koylu, Multi-objective optimization of operating parameters for a H2/Diesel dual-fuel compression-ignition engine, Int. J. Hydrog. Energy 45 (38) (2020) 19965–19975.

[58] Y. Srinivas, S.M. Mathew, A. Kothakota, N. Sagarika, R. Pandiselvam, Microwave assisted fluidized bed drying of nutmeg mace for essential oil enriched extracts: an assessment of drying kinetics, process optimization and quality, Innov. Food Sci. Emerg. Technol. 66 (2020), 102541.